162

FWI imaging: achieving AVA reflectivity faster than the conventional workflow

J. McLeman[1], T. Rayment[2], K. Dancer[1], T. Burgess[1]

[1] DUG Technology; [2] DUG Technology

Summary

Many seismic processing and imaging workflows have been developed over the years to attenuate aspects of the recorded wavefield which cannot be properly mapped into the image domain through conventional migration algorithms. These workflows, including techniques such as deghosting, designature, and demultiple, have become extensive and time-consuming to execute due to the linear-like fashion they must be applied. Each stage in the workflow must undergo a range of parameter testing with success judged on a subjective basis. We present the application of a novel multi-parameter full-waveform inversion (FWI) imaging technique as an alternative to the conventional workflow. It uses the raw field data to simultaneously perform model building and least squares imaging with all the recorded reflection wavefield. This approach uses the primaries, multiples, and ghosts to generate standard model parameters (like velocity and anisotropy) and high-resolution true amplitude AVA reflectivity images fit for structural and amplitude analysis faster than the conventional workflow. In this paper, we compare the FWI derived reflectivity-with-angle outputs to that of a standard Kirchhoff preSDM workflow to highlight the suitability of FWI imaging to directly supersede the conventional workflows.

Introduction

Full-waveform inversion (FWI) has become an industry-standard model building tool enabling the determination of high-resolution subsurface properties like the P-wave velocity. However, conventional applications of this method involve utilising only the diving waves which, due to geological constraints and limited maximum offsets, often restricts the maximum update to shallower depths than the target of interest. This limitation necessitates subsequent passes of reflection tomography to generate updates to the required depth. This is undesirable due to the need for data conditioning to enable high quality residual moveout picking. Further, the ray-based tomographic approach is limited in resolution and may fail in areas of complex geology. Therefore, the inclusion of reflections in FWI offers an attractive alternative that liberates us from such restrictions.

Including reflections in FWI provides an opportunity to derive an interpretable product together with velocity in a significantly shorter time than the conventional processing and imaging workflow. FWI uses the raw field data, which includes primaries, multiples, and ghosts to derive a high-resolution image in an iterative least-squares sense. Common approaches to achieve such results use reflections in a high frequency, single parameter FWI for velocity (Letki et al., 2019), or make use of an additional parameter in a cascaded or simultaneous sense as a "bin" to dump a representation of the scattering interfaces which is then discarded, to yield the interpretable model. The derivative of the interpretable model thus yields a pseudo-reflectivity image (Kalinicheva et al., 2020; Zhang et al., 2020). While these methods can produce excellent fast-track structural images, *a priori* assumptions about density limit their amplitude fidelity, as does the use of common internal amplitude normalisation schemes to overcome elastic effects and unknown features of the source wavelet.

These limitations can be overcome by instead separating the kinematic and dynamic components in the FWI kernel, obtaining an appropriate understanding of the true source wavelet, and using an augmented acoustic wave equation (McLeman et al., 2021). This approach simultaneously inverts for velocity and amplitude vs angle (AVA) related reflectivity, where the determined reflectivity is suitable for structural and amplitude analysis and the velocity model can be used to improve conventional imaging. The separation of the migration and tomographic terms in the FWI kernel is achieved through a wavenumber-domain preconditioner using scattering angle as a discriminator. The rate of convergence for the simultaneous inversion is accelerated, with multi-parameter scaling and crosstalk issues mitigated, using an advanced quasi-Newton adaptive gradient optimizer. The application of this approach to high frequency, simultaneously inverting for velocity and intercept-reflectivity, was shown by Rayment et al. (2022).

In this paper, we extend the work of Rayment et al. (2022) to demonstrate the applicability of this FWI imaging approach to generate higher angle AVA-related products up to 45 Hz using 3D TTI FWI with the augmented acoustic wave equation on a dataset from the Australian North-West Shelf. This is compared to AVA products obtained from a conventional processing and Kirchhoff imaging workflow.

Method

The dataset used to demonstrate the method was a dual-source towed streamer acquisition with 8 cables and 6 km maximum offset. This data was used to generate (simultaneously) a set of high-resolution models including P-wave velocity and true-amplitude reflectivity angle stacks using the visco-acoustic TTI FWI augmented wave-equation. AVA related properties are then derived from these angle stacks.

A vital step in determining the true-amplitude reflectivity was the appropriate estimation of the amplitude of the source wavelet. Approaches to determining a wavelet for FWI involving near-field hydrophones (NFH) or gun-array modelling will not ensure that the amplitude of the modelled and observed data in FWI will match. Such amplitude differences are traditionally circumvented by kinematic-only objective functions (Warner et al., 2013). However, when determining AVA related products from FWI, an incorrect source amplitude will result in the incorrect estimation of primary

amplitudes and the sub-optimal use of multiple energy. A moderate level of source variation was observed in this survey. Since NFH data were not available, a gun-array modelled signature was first obtained and then refined using a shot-by-shot least-squares inversion matching the direct arrival of the modelled and observed data, thus removing the wavelet amplitude ambiguity.

The initial velocity model used for this test was a smoothed legacy model to which diving wave only FWI was applied up to 16 Hz to a maximum depth of 2 km. The FWI imaging approach was then used to simultaneously invert for velocity and true-amplitude reflectivity angle stacks beginning at 16 Hz where only 1/8th of the available shots were used. As the inversion frequency was increased towards the final frequency of 45 Hz, the total number of input shots was increased until 1/4 of the total were used. While it has been shown that this technique can be readily extended to additionally invert for epsilon anisotropy (McLeman et al., 2022), anisotropy was not updated as part of this test.

Results

To compare with the FWI imaging results, a Kirchhoff 3D preSDM was run using the FWI imaging output velocity model with input of processed data bandlimited to a maximum frequency of 45 Hz. Angle stacks were generated from the output of the Kirchhoff migration for comparison to the FWI derived outputs. The conventional workflow took extensive project time to produce results. AVA synthetics were also computed using well information in order to assess the amplitude fidelity of the results.

Figures 1a), b), c) shows near, mid and far angle stacks generated by a Kirchhoff PreSDM with all of the available processed data as input and using the FWI derived velocity model. Figures 1d), e), f) shows the angle stacks generated directly from the FWI imaging approach simultaneously with velocity using only 1/4 of the raw shots as input. We can see that the amplitude trend with angle is very similar but there is a reduction in noise, particularly on the near stack, using the FWI imaging approach. Common challenges with the conventional workflow, such as residual near angle multiple, presents no issue at all for the FWI imaging approach. Since it is using the multiples in the inversion to determine the true subsurface reflectivity with angle, no multiple-adaption technology is required. The FWI imaging result shows no residual multiple, ghost, or signature energy and is zero-phased. Thus, the FWI imaging approach has handled designature, deghosting, demultiple, model building, and least-squares imaging in a single step and with a faster turnaround time than the conventional flow.

In order to quantitatively measure the amplitude fidelity of the results, AVA synthetics were also computed using well information. Figure 2 shows comparisons of the well synthetic modelled responses (black) to the Kirchhoff preSDM (blue) and FWI (red) responses for near, mid and far angle ranges. The Vp-Vs ratio and p-impedance derived from the well data are also shown in figure 2. Both the Kirchhoff and FWI responses show a good tie to the synthetic with the FWI responses accurately capturing the expected decrease in amplitude with increasing angle at the level highlighted. Figure 3a) and b) shows a near angle stack from the Kirchhoff preSDM and FWI imaging respectively. The synthetic overlay demonstrates a good tie to the FWI derived near-angle reflectivity. Thus, further highlighting the applicability of the FWI imaging approach to generating AVA-compliant solutions.

Conclusions

Generating angle stacks for AVA analysis using the conventional processing and imaging approach contains many serial steps, each of which contain parameter testing requiring many subjective judgements. The FWI imaging approach can automatically obtain higher-resolution angle stacks simultaneously with velocity, with less noise, in a much shorter time frame than the conventional flow. This is a result of using the full wavefield in an iterative least-squares imaging approach. Given that the new FWI imaging approach has demonstrated it can achieve better results in a shorter timeframe compared with the conventional method, this approach supersedes the established workflow and thus offers a new philosophy in the processing and imaging of seismic data.

Acknowledgements

We would like to thank Multi-Client Resources (MCR) for permission to use the Bex MC3D dataset and DUG Technology (DUG) for allowing us to present this work.

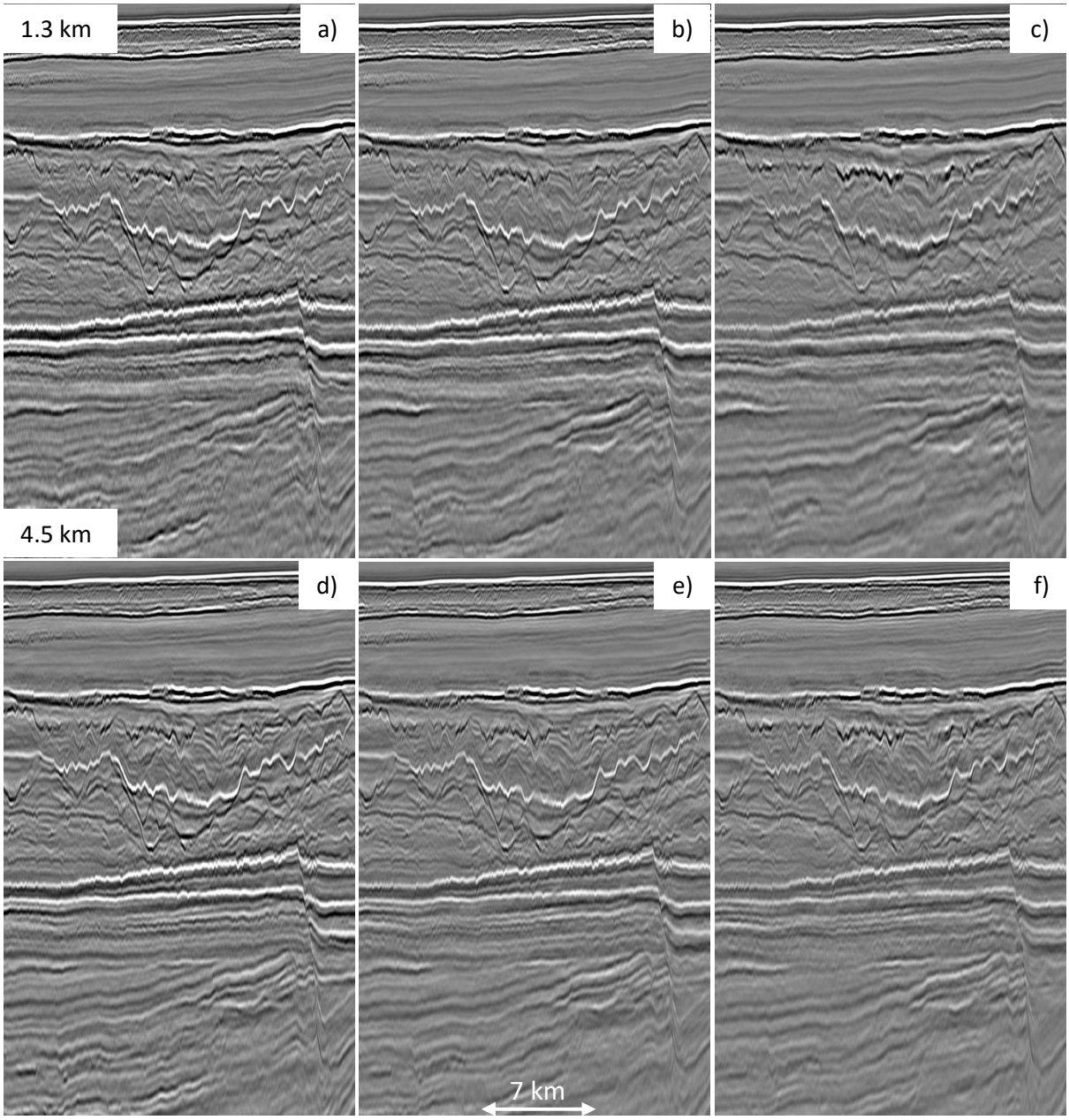

Figure 1: *a), b), c) near, mid and far angle stacks generated by the conventional workflow using Kirchhoff migration. FWI imaging angle stacks are shown in d), e), f).*

References

Letki, L., Lamont, M., and Thompson. T. [2019]. High frequency full waveform inversion as an interpretation solution, *The APPEA Journal*, **59**(2), 904-908.

Kalinicheva, T., Warner, M., and Mancini, F. [2020]. Full-bandwidth FWI, *90th Annual International Meeting, SEG*, Expanded Abstracts, 651-655.

McLeman, J., Burgess, T., Sinha, M., Hampson, G. and Thompson, T. [2021]. Reflection FWI with an augmented wave equation and quasi-Newton adaptive gradient scheme, *First International Meeting for Applied Geoscience & Energy*, Expanded Abstracts, 667-671.

McLeman, J., Burgess, T., Rayment, T. [2022]. FWI imaging with simultaneous anisotropy estimation, *83rd EAGE Conference and Exhibition 2022*, 1, 1-5.

Rayment, T., Dancer, K., McLeman, J., and Burgess, T. [2022]. High-Resolution FWI imaging – an Alternative to Conventional Processing, *83rd EAGE Conference and Exhibition 2022*, 1, 1-5.

Warner, M., Ratcliffe, A., Nangoo, T., Morgan, J., Umpleby, A., Shah, N., Vinje, V., Štekl, I., Guasch, L., Win, C., Conroy, G., and Bertrand, A. [2013]. Anisotropic 3D full-waveform inversion, *Geophysics*, **78**(2), R59-R80.

Zhang, Z., Wu, Z., Wei, Z., Mei, J., Huang, R., and Wang, P. [2020]. FWI imaging: Full-wavefield imaging through full-waveform inversion, *90th Annual International Meeting*, SEG, Expanded Abstracts, 656-660.

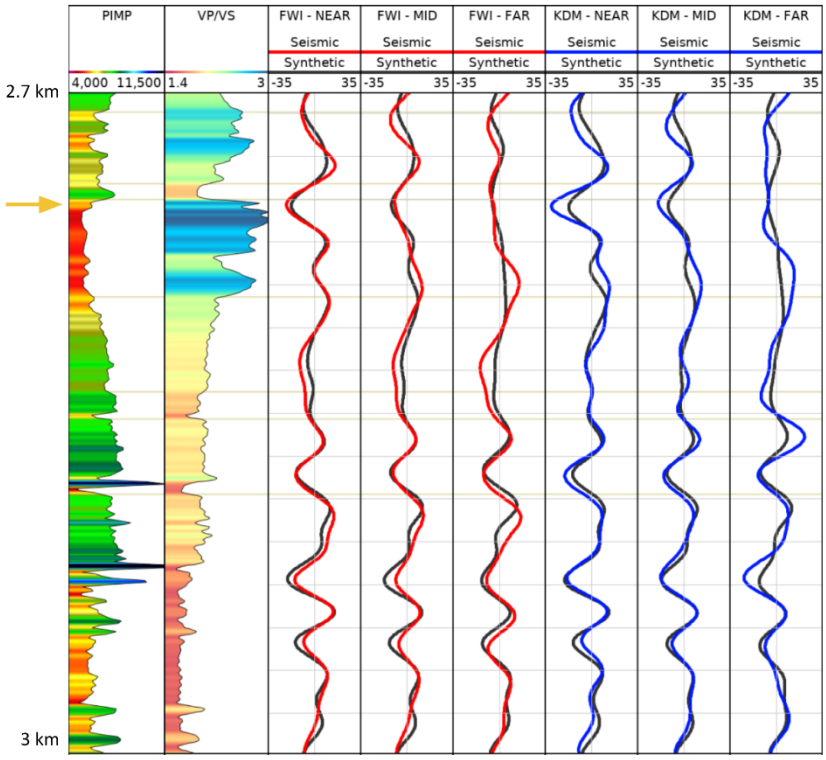

Figure 2: *Well logs and AVA synthetics (black) compared to FWI imaging (red) and Kirchhoff preSDM (blue) responses for near, mid and far angle ranges.*

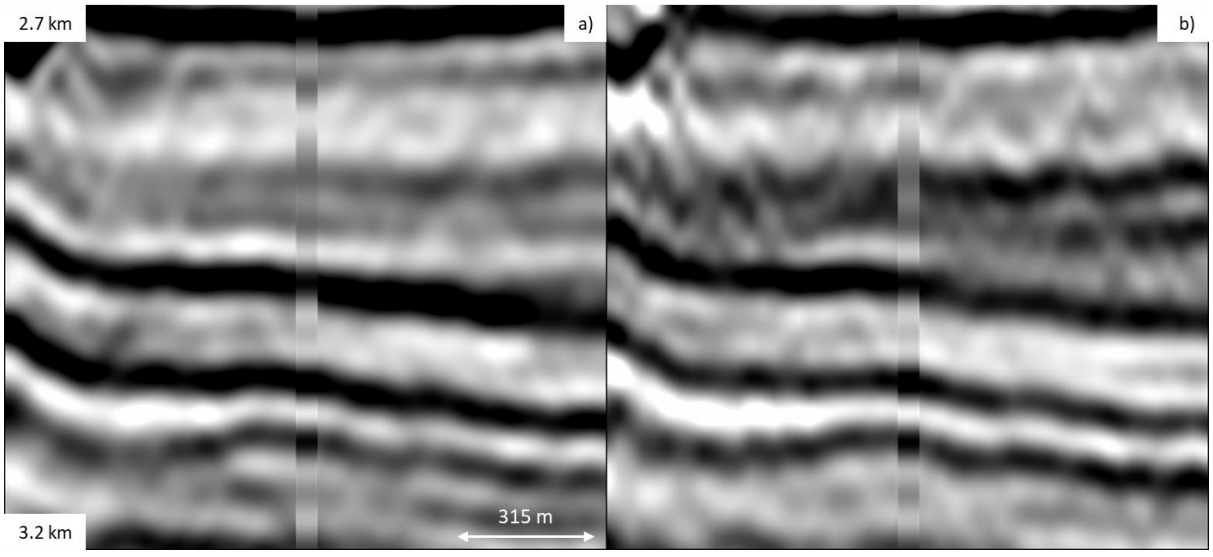

Figure 3: *Seismic section and synthetic overlay for (a) conventional Kirchhoff preSDM near stack, (b) FWI derived near stack.*